Advanced Steel Construction – Vol. 17 No. 2 (2021) 95–103
DOI:10.18057/IJASC.2021.17.2.1

EQUIVALENT PROPERTIES FOR ANALYSIS AS BEAM-COLUMN OF STEEL SPATIAL LATTICES OF RECTANGULAR CROSS-SECTION

Alberto M. Guzmán * and Victor A. Roldan

CeReDeTeC, Facultad Regional Mendoza, Universidad Tecnológica Nacional, Mendoza, Argentina
** (Corresponding author: E-mail: mguzman@frm.utn.edu.ar)*

ABSTRACT

Space lattices are widely used in various metal structural systems to form elements such as columns, beams, trusses, among others. These lattices are also used, for example, within the telecommunications industry to constitute the mast that supports the transmission devices. The spatial lattices have a large number of elements (legs, diagonals and struts). For its representation the equivalent beam-column model is very convenient, due to its low cost and computational effort. In previous studies, the author´s analyze of spatial lattice of triangular cross-section, have obtained continuous representation models from an energetic approach, as well as the equivalent properties for the modeling of lattice as beam-columns. Also adopting an energy approach, the study of four spatial lattice patterns of rectangular cross-section (Pattern 1, 2, 3 and 4) is carried out, obtaining the elastic properties and equivalent inertias necessary for the representation of the problem as column-beam. For the purpose of validating the proposed method, several numerical examples of spatial lattice implementing the beam-column model were evaluated. The results reached allow us to establish an excellent performance of the equivalent properties obtained for each of the lattices patterns considered, with the advantage of the low computational cost involved in its implementation, modeling and processing.

ARTICLE HISTORY

Received: 22 April 2020
Revised: 11 December 2020
Accepted: 12 December 2020

KEYWORDS

Spatial lattices;
Rectangular cross-section;
Beam-column;
Equivalent properties

1. Introduction

Spatial lattice structures are structures made up of a large number of simple elements such as legs, diagonals and struts. Due to this large number of elements that are part of the lattices, numerical modeling can involve significant computational effort and cost.

Several authors have developed and proposed continuous models for the representation of plane lattices, [1,2,3,4,5], while others, are based on an energetic approach, have developed continuous models for the representation of spatial lattices [6,7,8]. But the main research has been aimed at developing simplified representation models that allow less effort and computational cost at the time of structural analysis of spatial lattices. In this sense, we can cite [7] who developed a continuous 1D model for the representation of a spatial lattice of triangular cross-section used to support satellites solar panels. Or also the continuous 1D model developed by [9] for the dynamic, static and stability analysis of spatial lattices of triangular cross-section. Both indicated models were obtained from an energy statement.

As an alternative to the use of continuous 1D models, some authors have developed equivalent models for the discrete representation of spatial lattices [10,11,12]. In these developments, the equivalent elastic properties were obtained for the representation of the lattice as beam-column. In this particular case of what was developed by [9], equivalent elastic and inertia properties were obtained, allowing the dynamic and static analysis of spatial lattices of triangular cross- section. Four different lattice patterns were considered in the analysis.

These equivalent models of representation can be applied to various structural systems consisting of spatial lattices. For example, Páez and Sensale [13] analyzed a guyed mast against wind loads, modeling the mast as a beam-column and the guys as non-linear elastic springs. The equivalent properties adopted [14] corresponding only to elastic properties and without considering the rotational stiffness of the lattice.

The continuous 3D model presented by [8] was developed from an energetic approach, obtaining a system of 9 differential equations (9DE) for the representation of the structural behavior of a spatial lattice of triangular cross-section. From this model, [9] obtained a simplified 1D continuous model (6DE) by reducing the kinematics of the problem to the barycentric axis of the lattice.

As previously indicated, the developed models allow the representation of spatial lattices of triangular cross-section. For this reason and continuing with the developed energy methodology [9], the study of four spatial lattice patterns of rectangular cross-section (Pattern 1, 2, 3 and 4) is carried out, obtaining the elastic properties and equivalent inertias necessary for the representation of the problem as column-beam.

The interest in developing simplified models of representation of spatial lattices of rectangular cross-section, is mainly due to the fact that they are widely used to constitute various structural systems such as columns, beams, trusses, among others. (Fig. 1).

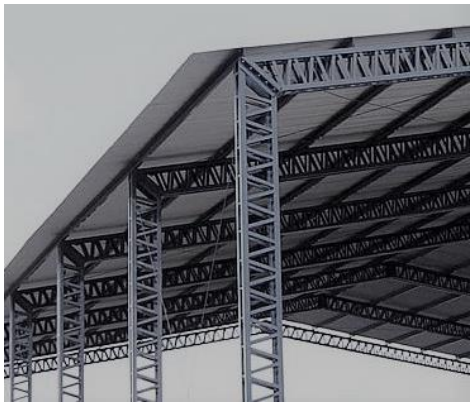

Fig. 1 Lattices of rectangular cross-section

In this way, the development of a simplified representation such that of the equivalent beam-column model, contributes to a significant time savings of modeling and computational processing of structural systems formed by lattices of rectangular cross-section.

2. Lattices analyzed

Four lattice patterns (Pattern 1, 2, 3 and 4) of rectangular cross-section of sides *B* and *D* are analyzed (Fig. 2).

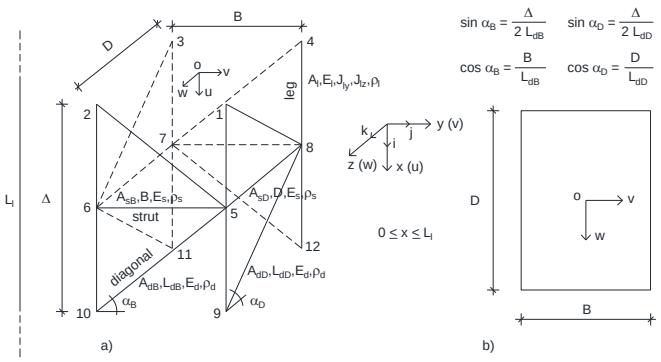

Fig. 2 Lattice analyzed. a) General view. b) Section view

Pattern 1 has zig-zag diagonals, Pattern 2 incorporates struts to the previous diagonalization, while Pattern 3 has double zig-zag diagonalization, and finally, Pattern 4 incorporates struts to the latter (Fig. 3).

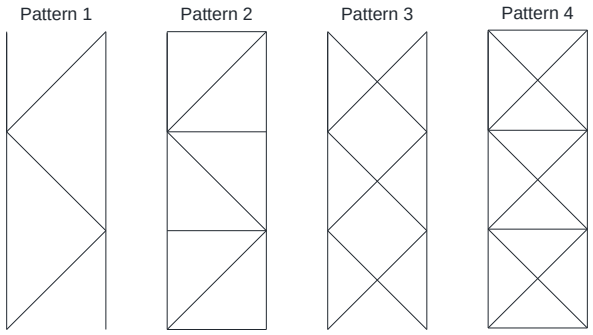

Fig. 3 Patterns considered

3. Energy approach for the analyzed spatial lattice

For the energy approach, it is initially considered that the spatial lattice is in an equilibrium configuration. When an external action acts upon it, it is deformed adopting a new equilibrium configuration. Given this, the lattice nodes experienced kinematically admissible displacements in the main directions. These displacements cause the elements that are part of the lattice to develop energy contributions [8].

From this approach, the energy expressions presented below, correspond to the energies developed by the elements (legs and diagonals) that are part of the spatial lattice of rectangular cross-section with a diagonal pattern of type Pattern 1 (Fig. 3).

3.1. Elastic deformation energy

$$U = \frac{1}{2}\frac{E_d A_{dB}}{L_{dB}\Delta}\int_0^{L_l}(A_{1B}sin^2\alpha_B + A_{2B}cos^2\alpha_B + A_{3B}sin\alpha_B cos\alpha_B)dx + \\ + \frac{1}{2}\frac{E_d A_{dD}}{L_{dD}\Delta}\int_0^{L_l}(A_{1D}sin^2\alpha_D + A_{2D}cos^2\alpha_D + A_{3D}sin\alpha_D cos\alpha_D)dx + \\ \frac{1}{2}E_l A_l\int_0^{L_l}A_4 dx + \frac{1}{2}E_l J_{ly}\int_0^{L_l}A_5 dx + \frac{1}{2}E_l J_{lz}\int_0^{L_l}A_6 dx \quad (1)$$

in which the coefficients are:

$$A_{1B} = 2\mathrm{u_j}(x,t)\mathrm{u_j}(x,t) - 4\big(\mathrm{u_a}(x,t)\mathrm{u_b}(x,t) + \mathrm{u_c}(x,t)\mathrm{u_d}(x,t)\big) + \\ + \frac{1}{2}\big(\mathrm{u_b'^2}(x,t) + \mathrm{u_d'^2}(x,t)\big)\Delta^2 \quad (2a)$$

$$A_{2B} = 2\mathrm{v_j}(x,t)\mathrm{v_j}(x,t) - 4\big(\mathrm{v_a}(x,t)\mathrm{v_b}(x,t) + \mathrm{v_c}(x,t)\mathrm{v_d}(x,t)\big) + \\ + \frac{1}{2}\big(\mathrm{v_b'^2}(x,t) + \mathrm{v_d'^2}(x,t)\big)\Delta^2 \quad (2b)$$

$$A_{3B} = 2\big[\big(\mathrm{u_a}(x,t) - \mathrm{u_b}(x,t)\big)v_b'(x,t) - \big(\mathrm{u_c}(x,t) - \mathrm{u_d}(x,t)\big)v_d'(x,t) + \\ \big(\mathrm{v_a}(x,t) - \mathrm{v_b}(x,t)\big)u_b'(x,t) - \big(\mathrm{v_c}(x,t) - \mathrm{v_d}(x,t)\big)u_d'(x,t)\big]\Delta \quad (2c)$$

$$A_{1D} = 2\mathrm{u_j}(x,t)\mathrm{u_j}(x,t) - 4\big(\mathrm{u_a}(x,t)\mathrm{u_d}(x,t) + \mathrm{u_b}(x,t)\mathrm{u_c}(x,t)\big) + \\ + \frac{1}{2}\big(\mathrm{u_a'^2}(x,t) + \mathrm{u_c'^2}(x,t)\big)\Delta^2 \quad (2d)$$

$$A_{2D} = 2\mathrm{w_j}(x,t)\mathrm{w_j}(x,t) - 4\big(\mathrm{w_a}(x,t)\mathrm{w_d}(x,t) + \mathrm{w_b}(x,t)\mathrm{w_c}(x,t)\big) + \\ + \frac{1}{2}\big(\mathrm{w_a'^2}(x,t) + \mathrm{w_c'^2}(x,t)\big)\Delta^2 \quad (2e)$$

$$A_{3D} = 2\big[\big(\mathrm{u_a}(x,t) - \mathrm{u_d}(x,t)\big)w_a'(x,t) - \big(\mathrm{u_b}(x,t) - \mathrm{u_c}(x,t)\big)w_c'(x,t) + \\ \big(\mathrm{w_a}(x,t) - \mathrm{w_d}(x,t)\big)u_a'(x,t) - \big(\mathrm{w_b}(x,t) - \mathrm{w_c}(x,t)\big)u_c'(x,t)\big]\Delta \quad (2f)$$

$$A_4 = u_j'(x,t)u_j'(x,t) \quad (2g)$$

$$A_5 = v_j''(x,t)v_j''(x,t) \quad (2h)$$

$$A_6 = w_j''(x,t)w_j''(x,t) \quad (2i)$$

where the notation has been used: $(\blacksquare)' \equiv \frac{\partial(\blacksquare)}{\partial x}$; $(\blacksquare)'' \equiv \frac{\partial^2(\blacksquare)}{\partial x^2}$; $j = a, b, c, d$

3.2. Energy by the external work of the acting loads

3.2.1. Sefl-weight

$$W_p = p_j \int_0^{L_l} u_j(x,t)dx \quad (3)$$

3.2.2. Concentrated loads acting on the legst

$$W_P = p_{uj}(t)u_j(x,t) + p_{vj}(t)v_j(x,t) + p_{wj}(t)w_j(x,t) \quad (4)$$

3.2.3. Distributed loads acting on the legst

$$W_q = \int_0^{L_l}\Big(q_{uj}(x,t)u_j(x,t) + q_{vj}(x,t)v_j(x,t) + q_{wj}(x,t)w_j(x,t)\Big)dx \quad (5)$$

3.2.4. Local moments acting on the legst

$$W_m = M_{vj}(t)w_j'(x,t) + M_{wj}(t)v_j'(x,t) \quad (6)$$

3.2.5. Second order effect by self-weight and by axial loads applied on the legs

$$W_{2^\circ} = \frac{1}{2}P_{uj}(t)\int_0^{L_l}\Big[\Big(v_j'(x,t)\Big)^2 + \Big(w_j'(x,t)\Big)^2\Big]dx + \\ + \frac{1}{2}p_j\ (t)\int_0^{L_l}\Big[\Big(v_j'(x,t)\Big)^2 + \Big(w_j'(x,t)\Big)^2\Big]xdx \quad (7)$$

where has been defined: $p_j = \rho_l g A_l + \frac{1}{2}\rho_d g\left(\frac{A_{dB}}{sin\alpha_B} + \frac{A_{dD}}{sin\alpha_D}\right)$

and the notation has been used: $(\blacksquare)' \equiv \frac{\partial(\blacksquare)}{\partial x}$; $(\blacksquare)'' \equiv \frac{\partial^2(\blacksquare)}{\partial x^2}$; $j = a, b, c, d$

3.3. Kinetic energy

$$T = \frac{1}{3}\rho_d A_{dB}\frac{L_{dB}}{\Delta}\int_0^{L_l}(B_{1B} + B_{2B})dx + \frac{1}{3}\rho_d A_{dD}\frac{L_{dD}}{\Delta}\int_0^{L_l}(B_{1D} + B_{2D})dx + \\ + \frac{1}{2}\rho_l A_l\int_0^{L_l}B_3 dx + \frac{1}{2}\rho_l J_{ly}\int_0^{L_l}B_4 dx + \frac{1}{2}\rho_l J_{lz}\int_0^{L_l}B_5 dx \quad (8)$$

in which the coefficients are:

$$B_{1B} = \dot{u}_j(x,t)\dot{u}_j(x,t) + \dot{v}_j(x,t)\dot{v}_j(x,t) + \dot{w}_j(x,t)\dot{w}_j(x,t) + \\ + \dot{u}_a(x,t)\dot{u}_b(x,t) + \dot{v}_a(x,t)\dot{v}_b(x,t) + \dot{w}_a(x,t)\dot{w}_b(x,t) + \\ + \dot{u}_c(x,t)\dot{u}_d(x,t) + \dot{v}_c(x,t)\dot{v}_d(x,t) + \dot{w}_c(x,t)\dot{w}_d(x,t) \quad (9a)$$

$$B_{2B} = \frac{1}{4}\big(\dot{u}_b'^2(x,t) + \dot{v}_b'^2(x,t) + \dot{w}_b'^2(x,t) + \dot{u}_d'^2(x,t) + \dot{v}_d'^2(x,t) + \\ + \dot{w}_d'^2(x,t)\big)\Delta^2 \quad (9b)$$

$$B_{1D} = \dot{u}_j(x,t)\dot{u}_j(x,t) + \dot{v}_j(x,t)\dot{v}_j(x,t) + \dot{w}_j(x,t)\dot{w}_j(x,t) + \\ + \dot{u}_a(x,t)\dot{u}_d(x,t) + \dot{v}_a(x,t)\dot{v}_d(x,t) + \dot{w}_a(x,t)\dot{w}_d(x,t) + \\ + \dot{u}_b(x,t)\dot{u}_c(x,t) + \dot{v}_b(x,t)\dot{v}_c(x,t) + \dot{w}_b(x,t)\dot{w}_c(x,t) \quad (9c)$$

$$B_{2D} = \frac{1}{4}\big(\dot{u}_a'^2(x,t) + \dot{v}_a'^2(x,t) + \dot{w}_a'^2(x,t) + \dot{u}_c'^2(x,t) + \dot{v}_c'^2(x,t) + \\ + \dot{w}_c'^2(x,t)\big)\Delta^2 \quad (9d)$$

where the notation has been used: $(\dot{\blacksquare}) \equiv \frac{\partial(\blacksquare)}{\partial t}$; $j = a, b, c, d$

It should be noted that if we apply the Hamilton's principle to the Lagrangian L of the system with the determined energy expressions, a continuous 3D model is obtained constituted of 12 differential equations (12DE) that represent the behavior of spatial lattice of rectangular cross-section.

But on the other hand, with the determined expressions as it will be seen in the next section, we obtain a simplified 1D continuous model of representation. This 1D model leads to obtaining the equivalent properties necessary for the representation of the lattice as a discrete beam-column model.

4. Continuous 1D model

The continuous 3D representation model for the spatial lattice of rectangular cross-section has particularity that of the 12 DE system coupled to each other, which makes its numerical resolution more complex. Given the fact that, a valid alternative for a simplified representation is the construction of a continuous 1D model. In this case, the model is made up of a 6 DE system, with

a simpler numerical resolution than that of the 3D model.

From this continuous 1D model and as previously stated, it is possible to obtain the equivalent properties necessary for the representation of the spatial lattice as a discrete beam-column model. This last form of representation constitutes the simplest model capable of numerically evaluating the mechanical behavior of spatial lattice, with a very low computational cost.

The development of a simplified 1D continuous model involves first defining a displacement field that allows the displacements of any point *P* located on the cross-section of the lattice (Fig. 4) to be related to the displacements experienced by the barycentric axis *o* of the section.

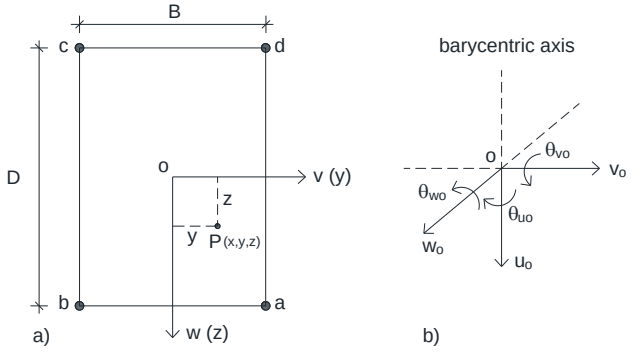

Fig. 4 a) Arbitrary point *P*. b) Sign convention (positive)

Thus, the displacement field is:

$$u(x,y,z,t) = u_o(x,t) - \theta_{wo}(x,t)y + \theta_{vo}(x,t)z$$
$$v(x,y,z,t) = v_o(x,t) - \theta_{uo}(x,t)z$$
$$w(x,y,z,t) = w_o(x,t) + \theta_{uo}(x,t)y \quad (10)$$

At this point, it has been assumed that displacements present linear variation and that torsional warping is not considered.

The six unknown functions represent:
. u_o (*x* direction) the axial displacement
. v_o and w_o (*y* and *z* directions, respectively) the transverse displacements
. θ_{uo} (around the *x* axis) the torsional slop
. θ_{vo} and θ_{wo} (around the *y* and *z* axes, respectively) the bending slopes
with which, the displacements of each leg can be expressed as follows:

$$u_a(x,t) = u_o(x,t) - \theta_{wo}(x,t)\frac{B}{2} + \theta_{vo}(x,t)\frac{D}{2}$$
$$u_b(x,t) = u_o(x,t) + \theta_{wo}(x,t)\frac{B}{2} + \theta_{vo}(x,t)\frac{D}{2}$$
$$u_c(x,t) = u_o(x,t) + \theta_{wo}(x,t)\frac{B}{2} - \theta_{vo}(x,t)\frac{D}{2}$$
$$u_d(x,t) = u_o(x,t) - \theta_{wo}(x,t)\frac{B}{2} - \theta_{vo}(x,t)\frac{D}{2}$$
$$v_a(x,t) = v_o(x,t) - \theta_{uo}(x,t)\frac{D}{2}$$
$$v_b(x,t) = v_o(x,t) - \theta_{uo}(x,t)\frac{D}{2}$$
$$v_c(x,t) = v_o(x,t) + \theta_{uo}(x,t)\frac{D}{2}$$
$$v_d(x,t) = v_o(x,t) + \theta_{uo}(x,t)\frac{D}{2}$$
$$w_a(x,t) = w_o(x,t) + \theta_{uo}(x,t)\frac{B}{2}$$
$$w_b(x,t) = w_o(x,t) - \theta_{uo}(x,t)\frac{B}{2}$$
$$w_c(x,t) = w_o(x,t) - \theta_{uo}(x,t)\frac{B}{2}$$
$$w_a(x,t) = w_o(x,t) + \theta_{uo}(x,t)\frac{B}{2} \quad (11)$$

Replacing these displacements obtained for the legs (Eqs. 11) in the energy expressions corresponding to the 3D model (Eqs. 1, 3 to 8), we obtain the energy expressions referring to the barycentric axis of the cross-section, that is, the energy expressions of the 1D model.

On the other hand the Lagrangian (L_o) of the simplified system results:

$$L_o = V_o - T_o \quad (12)$$

where $V_o = (U_o - W_o)$ and T_o are the potential and the kinetic energies, respectively, of 1D model. Whereas U_o is the elastic deformation energy, and W_o is the work of external loads.

Thus, applying the Hamilton's principle to the Lagrangian L_o (Eq. 12), we obtain a system of differential and linear equations (6DE) in the variables *x* and *t*, that represents the behavior of the lattice analyzed in the continuous domain (1D model).

$$(EA)_{o1}u_o''(x,t) - (\rho A)_{o1}\ddot{u}_o(x,t) + r_{do1}\ddot{u}_o''(x,t) - 4\big(p_o + q_{uo}(x,t)\big) = 0 \quad (13)$$

$$4E_lJ_{ly}v_o''(x,t) - (GA_B)_{o1}(v_o''(x,t) - \theta_{wo}'(x,t)) + 4(P_{uo}(t) + p_ox)v_o''(x,t) + 4p_ov_o'(x,t) + (\rho A)_{o1}\ddot{v}_o(x,t) - \big(4\rho_lJ_{ly} + r_{do1}\big)\ddot{v}_o''(x,t) - -q_{vo}(x,t) = 0 \quad (14)$$

$$4E_lJ_{lz}w_o''(x,t) - (GA_D)_{o1}(w_o''(x,t) + \theta_{vo}'(x,t)) + 4(P_{uo}(t) + p_ox)w_o''(x,t) + 4p_ow_o'(x,t) + (\rho A)_{o1}\ddot{w}_o(x,t) - (4\rho_lJ_{lz} + r_{do1})\ddot{w}_o''(x,t) - -4q_{wo}(x,t) = 0 \quad (15)$$

$$E_l\big(J_{ly}D^2 + J_{lz}B^2\big)\theta_{uo}''''(x,t) - (GJ_x)_{01} - [(P_{uo}(t) + p_ox)(D^2 + B^2)]\theta_{uo}''(x,t) + p_o(D^2 + B^2)\theta_{uo}'(x,t) + (\rho J_x)_{o1}\ddot{\theta}_{uo}(x,t) - \Big[\rho_l\big(J_{ly}D^2 + J_{lz}B^2\big) + \tfrac{1}{4}r_{do1}(D^2 + B^2)\Big]\ddot{\theta}_{uo}''(x,t) = 0 \quad (16)$$

$$\tfrac{1}{4}(EA)_{01}D^2\theta_{vo}''(x,t) - (GA_D)_{o1}\Big(w_o'(x,t) + \theta_{vo}(x,t)\Big) - (\rho J_{xD})_{o1}\ddot{\theta}_{vo}(x,t) + + \tfrac{1}{4}r_{do1}D^2\ddot{\theta}_{vo}''(x,t) - \tfrac{1}{2}(A_{dD}sin^3\alpha_D - A_{dB}sin^3\alpha_B)BD\theta_{wo}''(x,t) - - \tfrac{1}{48}\rho_d\left(\tfrac{A_{dD}}{sin\alpha_D} - \tfrac{A_{dB}}{sin\alpha_B}\right)BD\Delta^2\ddot{\theta}_{wo}''(x,t) = 0 \quad (17)$$

$$\tfrac{1}{4}(EA)_{01}B^2\theta_{wo}''(x,t) - (GA_B)_{o1}\Big(v_o'(x,t) - \theta_{wo}(x,t)\Big) - (\rho J_{xB})_{o1}\ddot{\theta}_{wo}(x,t) + + \tfrac{1}{4}r_{do1}B^2\ddot{\theta}_{wo}''(x,t) - \tfrac{1}{2}(A_{dD}sin^3\alpha_D - A_{dB}sin^3\alpha_B)BD\theta_{vo}''(x,t) - - \tfrac{1}{48}\rho_d\left(\tfrac{A_{dD}}{sin\alpha_D} - \tfrac{A_{dB}}{sin\alpha_B}\right)BD\Delta^2\ddot{\theta}_{vo}''(x,t) = 0 \quad (18)$$

The introduced notation $(EA)_{o1}$, $(GAB)_{o1}$, $(GAD)_{o1}$, $(GJx)_{o1}$, $(\rho A)_{o1}$, $(\rho Jx)_{o1} = (\rho J_{xD})_{o1} + (\rho J_{xB})_{o1}$ and r_{do1}, correspond to the equivalent beam-column properties presented in the following section. The subscript *o* represents the reference with respect to the barycentric axis of the cross-section, while subscript *1* represents the type of diagonalization pattern analyzed.

5. Equivalent properties for the beam-column model

The notation introduced in the expressions of the differential system (Eqs. 13 to 18) represents the beam-column equivalent properties corresponding to Pattern 1, which result:

$$(EA)_{01} = 4E_lA_l + \tfrac{1}{2}E_d(A_{dD}sin^3\alpha_D + A_{dB}sin^3\alpha_B) \quad (19)$$

$$(GA_B)_{01} = 2E_dA_{dB}sin\alpha_Bcos^2\alpha_B \quad (20)$$

$$(GA_D)_{01} = 2E_dA_{dD}sin\alpha_Dcos^2\alpha_D \quad (21)$$

$$(GJ_x)_{01} = \tfrac{1}{4}((GA_B)_{01}D^2 + (GA_D)_{01}B^2) \quad (22)$$

$$(\rho A)_{01} = 4\rho_lA_l + 2\rho_d\left(\tfrac{A_{dD}}{sin\alpha_D} + \tfrac{A_{dB}}{sin\alpha_B}\right) \quad (23)$$

$$(\rho J_x)_{01} = (\rho J_{xB})_{01} + (\rho J_{xD})_{01} \quad (24)$$

$$(\rho J_{xB})_{01} = \left[\rho_lA_l + \tfrac{1}{6}\rho_d\left(3\tfrac{A_{dD}}{sin\alpha_D} + \tfrac{A_{dB}}{sin\alpha_B}\right)\right]B^2 \quad (25)$$

$$(\rho J_{xD})_{01} = \left[\rho_lA_l + \tfrac{1}{6}\rho_d\left(\tfrac{A_{dD}}{sin\alpha_D} + 3\tfrac{A_{dB}}{sin\alpha_B}\right)\right]D^2 \quad (26)$$

$(EA)_{o1}$, $(GA_B)_{o1}$, $(GA_D)_{o1}$ and $(GJ_x)_{o1}$ are the axial, shear (directions *y* and *z*) and torsional stiffness, while $(\rho A)_{o1}$ is the translational inertia and $(\rho J_x)_{o1} = (\rho J_{xD})_{o1} + (\rho J_{xB})_{o1}$ is the global torsional inertia of the system (Pattern 1) with respect to the centroid axis. Regarding the term r_{do1}, it is related to the inertial contribution of the diagonals:

$$r_{d01} = \frac{1}{6}\rho_d \left(\frac{A_{dD}}{sin\alpha_D} + \frac{A_{dB}}{sin\alpha_B}\right)\Delta^2 \quad (27)$$

On the other hand, the relationship between $\theta_{wo}(x,t)$ and $v_o(x,t)$, and between $\theta_{vo}(x,t)$ and $w_o(x,t)$, allow the definition of the following expressions:

$$\left(EJ_y\right)_{01} = 4E_lJ_{ly} + \frac{1}{4}(EA)_{01}B^2 \quad (28)$$

$$(EJ_z)_{01} = 4E_lJ_{lz} + \frac{1}{4}(EA)_{01}D^2 \quad (29)$$

$$\left(\rho J_y\right)_{01} = 4\rho_lJ_{ly} + (\rho J_{xB})_{01} + \frac{1}{4}(\rho A)_{01}\frac{(EA)_{01}}{(GA_B)_{01}}B^2 + r_{d01} \quad (30)$$

$$(\rho J_z)_{01} = 4\rho_lJ_{lz} + (\rho J_{xD})_{01} + \frac{1}{4}(\rho A)_{01}\frac{(EA)_{01}}{(GA_D)_{01}}D^2 + r_{d01} \quad (31)$$

$(EJ_y)_{o1}$ and $(EJ_z)_{o1}$ are bending stiffness, and $(\rho J_y)_{o1}$ and $(\rho J_z)_{o1}$ are the global bending inertias with respect to the barycentric axis. Thus, expressions 19 to 31 result to be the equivalent properties necessary for the simplified modeling of the lattice as beam-column.

Following a similar mathematical development, the equivalent properties for other three diagonal patterns (Pattern 2, 3 and 4) have been derived. These will be presented in a corresponding section.

Therefore, the equivalent properties determined (elastic and inertial) for each of the diagonalization patterns analyzed (Pattern 1, 2, 3 and 4), allow to implement the simplified beam-column model for the static and dynamic evaluation of rectangular cross-section spatial lattices.

6. Implementation of the equivalent beam-column properties

6.1. Lattice column

Fig. 5 shows the lattice column (Pattern 1) to be analyzed using the equivalent beam-column (BC) model and under different boundary conditions (Fig. 6).

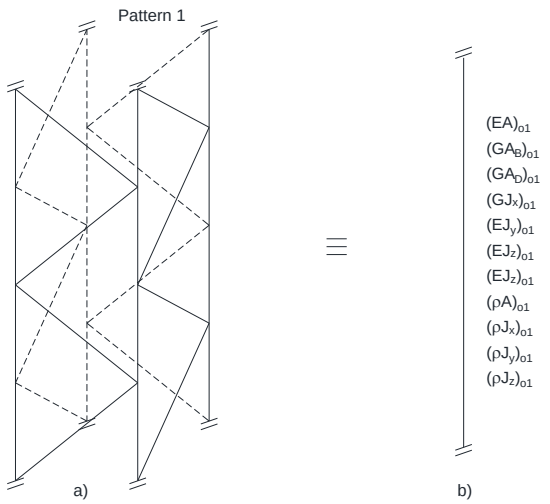

Fig. 5 Lattice column under study. a) SL-FEM model. b) BC-FEM model

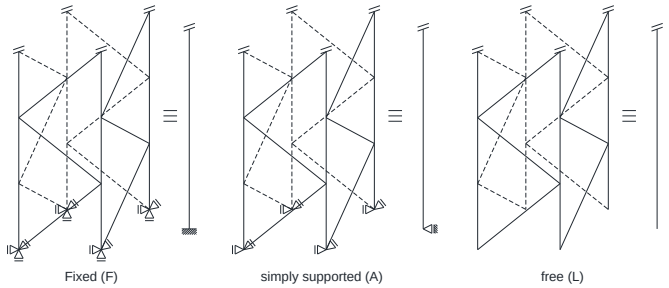

Fig. 6 Boundary conditions

For the sake of comparison, the spatial lattice is modeled with the finite element method (FEM) using a full 3D model denoted SL-FEM. Each leg is modeled using two-node beam elements, and two-node truss elements to represent the diagonals. The second FEM model named BC-FEM consist of a one dimensional beam-column representation of the lattice with equivalent properties obtained, using 6 two-node beam elements. The model was solved using the software SAP2000 [15], and the the results from static deflection and natural frequencies were compared.

The geometric and mechanical properties of the lattice analyzed are indicated in Table 1, while the equivalent beam-column properties are indicated in Table 2.

As applied loads, a transverse load is considered uniformly distributed in the *y* and *z* directions of value $q_{vo} = q_{wo} = 200$ N/m, and an axial load of value $P_{uo} = 1000$ N.

Table 1
Numerical values of geometrical and mechanical properties of the analyzed lattice

Parameter	Notation	Value	Unit
Leg length	L_l	6.0	m
Diagonals separation seseparation	Δ	0.4	m
Side B	B	0.2	m
Side D	D	0.4	m
Area of legs	A_l	$2.01\text{x}10^{-4}$	m^2
Area 2nd moment of legs	$J_{ly} = J_{lz}$	$3.22\text{x}10^{-9}$	m^4
Area of diagonals side B	A_{dB}	$5.03\text{x}10^{-5}$	m^2
Area of diagonals side D	A_{dD}	$1.13\text{x}10^{-4}$	m^2
Modulus of elasticity	$E_l = E_d$	200000	MPa
Mass density	$\rho_l = \rho_d$	7850	kg/m^3

Table 2
Beam-column equivalent properties for analyzed lattice

Properties	Notation	Value	Unit
Axial stiffnes (direction x)	$(EA)_{o1}$	$1.64\text{x}10^{8}$	N
Shear stiffnes (direction y) seseparation	$(GA_B)_{o1}$	$7.11\text{x}10^{6}$	N
Shear stiffnes (direction z)	$(GA_D)_{o1}$	$1.62\text{x}10^{7}$	N
Torsional stiffnes (around the x axis)	$(GJ_x)_{o1}$	$4.46\text{x}10^{5}$	$N.m^2$
Bending stiffnes (around the z axis)	$(EJ_y)_{o1}$	$1.64\text{x}10^{6}$	$N.m^2$
Bending stiffnes (around the y axis)	$(EJ_z)_{o1}$	$6.55\text{x}10^{6}$	$N.m^2$
Translational inertia (direction x)	$(\rho A)_{o1}$	$1.14\text{x}10^{1}$	kg/m
Torsional inertia (around the x axis)	$(\rho J_x)_{o1}$	$4.57\text{x}10^{-1}$	kg.m
Bending inertia (around the z axis)	$(\rho J_y)_{o1}$	2.80	kg.m
Bending inertia (around the y axis)	$(\rho J_z)_{o1}$	5.03	kg.m
Inertial contribution of the diagonals	r_{do1}	$6.78\text{x}10^{-2}$	kg.m

The results obtained by implementing the different models (SL-FEM and BC-FEM) are reported, allowing to establish the performance of the BC-FEM model developed.

Table 3 and 4 shows respectively the obtained values of the maximum lateral displacement in the *y* ($v_{o(max)}$) and *z* ($w_{o(max)}$) directions, for the different boundary conditions. Table 5 shows the obtained values of the maximum axial displacement in the *x* direction ($u_{o(max)}$), and Table 6 shows the results obtained of the first circular frequencies for axial and bending mode types (denoted with superscripts *a* and *b* respectively).

Table 3
Static deflection case. Maximum transverse displacements in direction *y*

Boundary condition	$v_{o(max)}$ [mm]		
	SL-FEM	BC-FEM	Difference [%]
A-A	2.228	2.186	1.92
F-F	0.552	0.538	2.60
F-A	1.024	1.002	2.20
F-L	20.635	20.276	1.77

Table 4
Static deflection case. Maximum transverse displacements in direction *z*

Boundary condition	$w_{o(max)}$ [mm]		
	SL-FEM	BC-FEM	Difference [%]
A-A	0.583	0.571	2.10
/BF-F	0.164	0.159	3.14
F-A	0.286	0.278	2.88
F-L	5.260	5.170	1.74

Table 5
Static deflection case. Maximum axial displacements

Boundary condition	$u_{o(max)}$ [mm]		
	SL-FEM	BC-FEM	Difference [%]
A-A			
F-F	0.0373	0.0367	1.63
F-A			
F-L	-	-	-

Table 6
Natural vibrations case. First natural frequency (a: axial; b_v: bending in y; b_w: bending in z)

Boundary condition	1st frequency [rad/seg]			
	mode	SL-FEM	BC-FEM	Difference [%]
A-A	ω_{1a}	312.871	312.171	0.22
	ω_{1bv}	15.866	16.034	1.05
	ω_{1bw}	30.921	31.338	1.33
F-F	ω_{1a}	313.051	312.171	0.28
	ω_{1bv}	32.146	32.557	1.26
	ω_{1bw}	58.973	59.732	1.27
F-A	ω_{1a}	156.523	157.447	0.59
	ω_{1bv}	23.530	23.632	0.43
	ω_{1bw}	44.464	44.761	0.66
F-L	ω_{1a}	156.404	157.432	0.65
	ω_{1bv}	5.750	5.737	0.23
	ω_{1bw}	11.351	11.346	0.04

The *Δ* step between diagonals is a necessary parameter for the passage from the discrete domain to the continuous domain of the energy terms provided by the diagonals and legs [8].

Consequently, the determination of the proposed equivalent properties depends on this passage previously indicated. Therefore, a spatial lattice (Pattern 1) of square cross-section is analyzed using different *Δ* values. This allows to establish its influence on the numerical results obtained using the BC-FEM model with 6 two-nodes beam elements. For the indicated analysis, *Δ*/side ratios (side B or D) are adopted between 0.25 and 2.00 (Fig. 7). The geometric and mechanical properties of the lattice analyzed are indicated in Table 7. The loads applied correspond to the same as in the previous case.

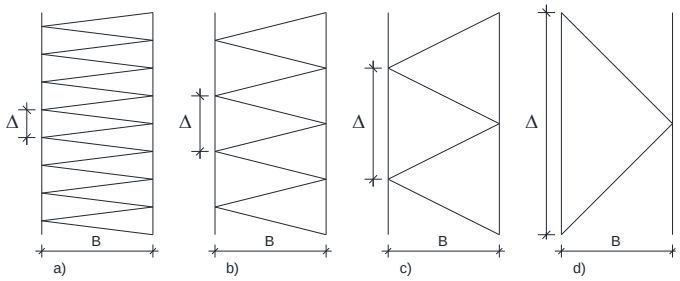

Fig. 7 a) Δ/B = 0.25. b) Δ/B = 0.50. c) Δ/B = 1.00. d) Δ/B = 2.00

Table 7
Properties of the analyzed lattice for different values Δ

Parameter	Notation	Value	Unit
Leg length	L_l	6.0	m
Diagonals separation seseparation	Δ	0.1;0.2;0.4;0.8	m
Side	B = D	0.4	m
Area of legs	A_l	$2.01x10^{-4}$	m^2
Area 2nd moment of legs	$J_{ly} = J_{lz}$	$3.22x10^{-9}$	m^4
Area of diagonals	$A_{dB} = A_{dD}$	$1.13x10^{-4}$	m^2
Modulus of elasticity	$E_l = E_d$	200000	MPa
Mass density	$\rho_l = \rho_d$	7850	kg/m^3

The results of the maximum transverse displacements obtained for different Δ/B ratios are presented in Tables 8 to 11.

Table 8
Case A-A. Maximum transverse displacements

Boundary condition	Δ/B	$v_{o(max)}$ [mm]		
		SL-FEM	BC-FEM	Difference [%]
A-A	0.25	0.687	0.687	0.00
	0.50	0.610	0.610	0.00
	1.00	0.568	0.573	0.87
	2.00	0.535	0.543	1.47

Table 9
Case F-F. Maximum transverse displacements

Boundary condition	Δ/B	$v_{o(max)}$ [mm]		
		SL-FEM	BC-FEM	Difference [%]
F-F	0.25	0.268	0.268	0.00
	0.50	0.192	0.192	0.00
	1.00	0.159	0.159	0.00
	2.00	0.156	0.156	0.00

Table 10
Case F-A. Maximum transverse displacements

Boundary condition	Δ/B	$v_{o(max)}$ [mm]		
		SL-FEM	BC-FEM	Difference [%]
F-A	0.25	0.405	0.404	0.25
	0.50	0.317	0.318	0.31
	1.00	0.278	0.277	0.36
	2.00	0.268	0.272	1.47

Table 11
Case F-L. Maximum transverse displacements

Boundary condition	Δ/B	$v_{o(max)}$ [mm]		
		SL-FEM	BC-FEM	Difference [%]
F-L	0.25	5.683	5.682	0.02
	0.50	5.363	5.372	0.17
	1.00	5.137	5.194	1.10
	2.00	4.825	5.021	3.90

Finally, the performance of the BC-FEM model is evaluated for different discretizations of the finite beam elements that are part of it. For this purpose, the example of the previous case corresponding to the ratio *Δ*/*B* = 1.00 and the boundary condition F-L is taken. The discretizations evaluated correspond to a number of frames between L_l/L_l and $L_l/0.01$ (L_l: height lattice). Tables 12 to 15 show the results obtained from the evaluation.

Table 12
Performance of the BC-FEM model for different discretization's. Case F-L. Maximum axial displacements

$u_{o(max)}$ [mm]				
Discretization	n° frame	SL-FEM	BC-FEM	Difference [%]
L_l/L_l	1	0.0365	0.0368	0.82
$L_l/1$	6		0.0368	0.82
$L_l/0.1$	60		0.0368	0.82
$L_l/0.01$	600		0.0368	0.82

Table 13
Performance of the BC-FEM model for different discretization's. Case F-L. Maximum transverse displacements

$u_{o(max)}$ [mm]				
Discretization	n° frame	SL-FEM	BC-FEM	Difference [%]
L_l/L_l	1	5.137	5.194	1.10
$L_l/1$	6		5.194	1.10
$L_l/0.1$	60		5.194	1.10
$L_l/0.01$	600		5.194	1.10

Table 14
Performance of the BC-FEM model for different discretization's. Case F-L. First natural frequency axial

$u_{o(max)}$ [mm]				
Discretization	n° frame	SL-FEM	BC-FEM	Difference [%]
L_l/L_l	1	141.689	126.812	11.73
$L_l/1$	6		140.451	0.88
$L_l/0.1$	60		140.849	0.60
$L_l/0.01$	600		140.853	0.59

Table 15
Performance of the BC-FEM model for different discretizations. Case F-L. First natural frequency bending

$u_{o(max)}$ [mm]				
Discretization	n° frame	SL-FEM	BC-FEM	Difference [%]
L_l/L_l	1	10.269	7.203	42.57
$L_l/1$	6		10.124	1.43
$L_l/0.1$	60		10.246	0.22
$L_l/0.01$	600		10.247	0.21

The internal forces in each element of the lattice (legs, diagonals) are easily obtained after knowing the efforts of the BC-FEM model.

Knowing the bending moment and the normal effort acting in a certain section of the BC, the axial efforts in the legs are obtained.

Being for example, $M_{\theta wo}(x)$ (bending moment around the axis w_o), $M_{\theta vo}(x)$ (bending moment around the axis v_o), and $N_{uo(x)}$ (normal effort in the direction u_o) the forces acting in the beam-column (BC) at a height x, the axial effort in each leg then results:

$$N_l = \frac{N_{uo}(x)}{4} + \frac{M_{\theta wo}(x)}{2B} + \frac{M_{\theta vo}(x)}{2D} \tag{32}$$

taking into account in this determination the sign that corresponds to each effort and the location of the leg.

Knowing the shear effort acting in the BC, the axial forces in the diagonals are obtained. For example, $S_{vo}(x)$ (shear effort in the direction of the v_o axis) and $S_{wo}(x)$ (shear effort in the direction of the w_o axis) acting in the BC at a height x, the axial effort in each diagonal then results:

$$N_{dB} = \frac{S_{vo}(x)}{2cos\alpha_B} \tag{33}$$

$$N_{dD} = \frac{S_{wo}(x)}{2cos\alpha_D} \tag{34}$$

In this way, from the efforts obtained in the BC-FEM representation model, the internal forces acting on each of the elements of the spatial lattice are recovered.

Taking the previous example corresponding to the relation $\Delta/B = 1.00$, with a discretization $L_l/1$, with F-L boundary conditions, and with a lateral load uniformly distributed in the direction of y of value $q_{vo} = 200$ N/m.

In this case, the efforts in the BC-FEM representation model and in the x section result $M_{\theta wo}(x) = 3373$ N.m and $S_{vo}(x) = 1160$ N.

Fig. 8 shows the elements of the SL-FEM evaluated.

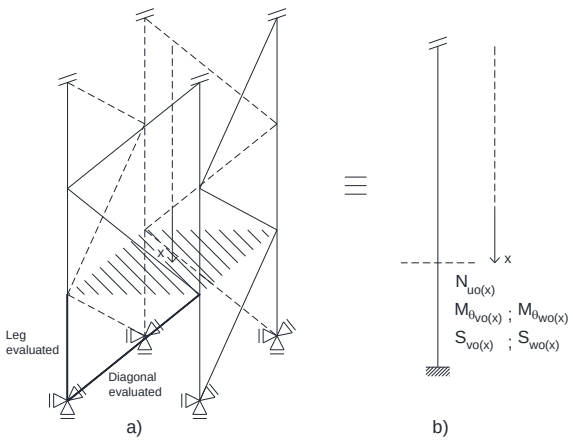

Fig. 8 Determination of internal efforts. a) SL-FEM. b) BC-FEM

Table 16 compares the internal efforts for the diagonal and leg evaluated, obtained in the SL-FEM model and from the resulting efforts in the BC-FEM model applying the Eqs. 32 to 34.

Table 16
Internal efforts in elements of spatial lattice. Case F-L

Internal efforts [N]				
Element	Effort	SL-FEM	BC-FEM	Difference [%]
Leg	Axial N_l	4117	4226	2.35
Diagonal	Axial N_d	663	649	2.16

6.2. Lattice frame

Fig. 9 shows the case of a lattice frame analyzed using the equivalent beam-column (BC). This is subject to a 2000 N/m vertical uniformly distributed load on the beam. The lattice frame is represented by the SL-FEM (Fig. 9a) and BC-FEM (Fig. 9b) models, comparing the numerical results for the maximum vertical deformation and for the first natural frequencies.

It should be noted that in the SL-FEM model 508 finite elements were used for the discretization of the problem, while in the BC-FEM model only 24 elements were used, which is, less than 5 % of what was used in the spatial model.

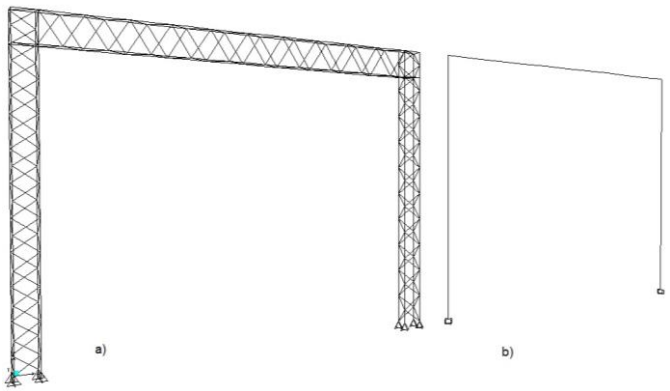

Fig. 9 Lattice frame. a) SL-FEM space model. b) BC-FEM equivalent model

The geometric and mechanical properties are indicated in Table 17.

Table 17
Numerical values of geometrical and mechanical properties of the lattice frame

Element	Parameter	Notation	Value	Unit
Column	Leg length	L_l	7.35	m
	Diagonals separation	D	0.7	m
	Side B	B	0.5	m
	Side D	D	0.3	m
	Area of legs	A_l	$2.01x10^{-4}$	m^2
	Area 2nd moment of legs	$J_{ly} = J_{lz}$	$3.22x10^{-9}$	m^4
	Area of diagonals side B	A_{dB}	$1.13x10^{-4}$	m^2
	Area of diagonals side D	A_{dD}	$5.03x10^{-5}$	m^2
	Modulus of elasticity	$E_l = E_d$	200000	MPa
	Mass density	$\rho_l = \rho_d$	7850	kg/m^3
Beam	Leg length	L_l	9.0	m
	Diagonals separation	D	0.9	m
	Side B	B	0.7	m
	Side D	D	0.3	m
	Area of legs	A_l	$2.01x10^{-4}$	m^2
	Area 2nd moment of legs	$J_{ly} = J_{lz}$	$3.22x10^{-9}$	m^4
	Area of diagonals side B	A_{dB}	$1.13x10^{-4}$	m^2
	Area of diagonals side D	A_{dD}	$5.03x10^{-5}$	m^2
	Modulus of elasticity	$E_l = E_d$	200000	MPa
	Mass density	$\rho_l = \rho_d$	7850	kg/m^3

Table 18 demonstrates the values obtained for the maximum vertical deformation of the beam, while Table 19 demonstrates the values for the first bending frequencies (transverse to the plane and longitudinal to this) and the torsional frequency of the lattice frame.

Table 18
Static deflection case. Maximum vertical displacement of the beam

Boundary condition	Vertical displacement [mm]		
	SL-FEM	BC-FEM	Difference [%]
F-F	7.790	7.632	2.07

Table 19
Natural vibrations case. First natural frequencies bending and torsional (b: bending; t: torsional)

Boundary condition	1st frequency [rad/seg]			
	mode	SL-FEM	BC-FEM	Difference [%]
F-F	$\omega_{1b(transverse)}$	3.155	3.079	2.47
	$\omega_{1b(longitudinal)}$	8.319	8.430	1.33
	$\omega_{1t(torsional)}$	5.014	5.153	2.77

Finally, the Figs. 10 to 13 show each of the evaluated responses.

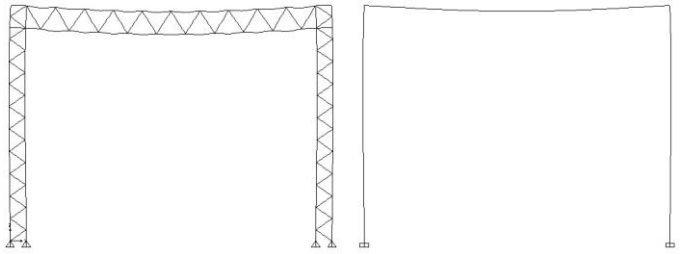

Fig. 10 Static deflection case. Maximum vertical displacement of the beam

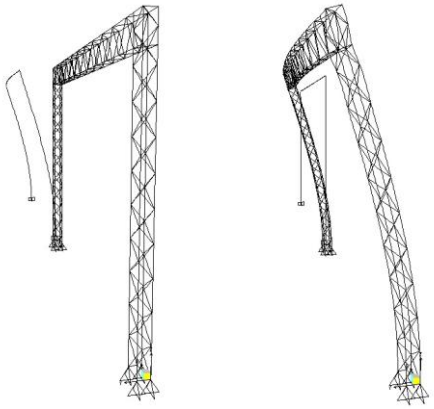

Fig. 11 Natural vibrations case. First bending frequency transverse to the plane of the lattice frame

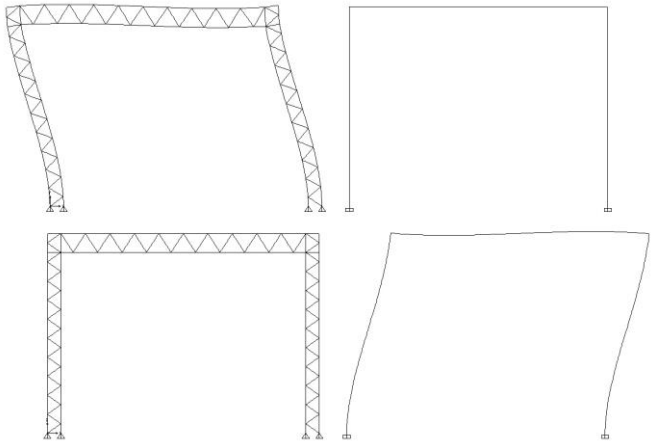

Fig. 12 Natural vibrations case. First bending frequency longitudinal to the plane of the lattice frame

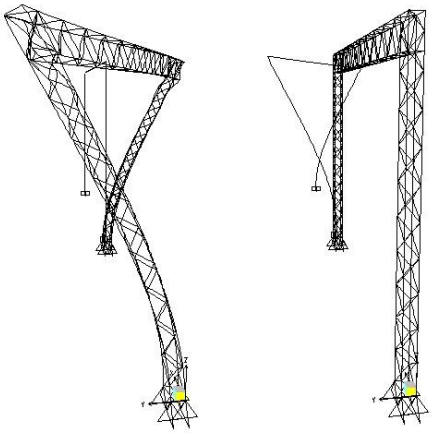

Fig. 13 Natural vibrations case. First torsional frequency of the lattice frame

7. Equivalent properties for different patterns

With mathematical statements similar to those suggested for the lattice structure (Pattern 1) described above, three other patterns were analyzed (Pattern 2, 3 and 4). New differential equations are stated resulting in the corresponding equivalent properties. Table 18 shows the obtained equivalent properties. The parameters with subscripts *s* represent the contributions of the struts for Pattern 2 and Pattern 4.

Table 20
Equivalent properties. Rectangular cross-sectional lattice

Equivalent properties	Pattern 1	Pattern 2
	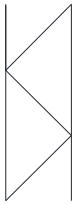	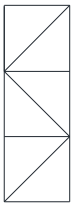
$(EA)_0$	$4E_lA_l + \frac{1}{2}E_d(A_{dB}sin^3\alpha_B + A_{dD}sin^3\alpha_D)$	$4E_lA_l + \frac{1}{2}E_d(A_{dB}sin^3\alpha_B + A_{dD}sin^3\alpha_D)$
$(GA_B)_0$	$2E_dA_{dB}sin\alpha_Bcos^2\alpha_B$	$2E_dA_{dB}sin\alpha_Bcos^2\alpha_B$
$(GA_D)_0$	$2E_dA_{dD}sin\alpha_Dcos^2\alpha_D$	$2E_dA_{dD}sin\alpha_Dcos^2\alpha_D$
$(GJ_x)_0$	$\frac{1}{4}((GA_B)_oD^2 + (GA_D)_oB^2)$	$\frac{1}{4}((GA_B)_oD^2 + (GA_D)_oB^2)$
$(\rho A)_0$	$4\rho_lA_l + 2\rho_d\left(\frac{A_{dD}}{sin\alpha_D} + \frac{A_{dB}}{sin\alpha_B}\right)$	$4\rho_lA_l + 2\rho_d\left(\frac{A_{dD}}{sin\alpha_D} + \frac{A_{dB}}{sin\alpha_B}\right) + 2\rho_s\left(\frac{A_{sD}}{tan\alpha_D} + \frac{A_{sB}}{tan\alpha_B}\right)$
$(\rho J_x)_0$	$(\rho J_{xD})_o + (\rho J_{xB})_o$	$(\rho J_{xD})_o + (\rho J_{xB})_o$
$(\rho J_{xD})_0$	$\left[\rho_lA_l + \frac{1}{6}\rho_d\left(\frac{A_{dD}}{sin\alpha_D} + 3\frac{A_{dB}}{sin\alpha_B}\right)\right]D^2$	$\left[\rho_lA_l + \frac{1}{6}\rho_d\left(\frac{A_{dD}}{sin\alpha_D} + 3\frac{A_{dB}}{sin\alpha_B}\right) + \frac{1}{6}\rho_s\left(\frac{A_{sD}}{tan\alpha_D} + 3\frac{A_{sB}}{tan\alpha_B}\right)\right]D^2$
$(\rho J_{xB})_0$	$\left[\rho_lA_l + \frac{1}{6}\rho_d\left(3\frac{A_{dD}}{sin\alpha_D} + \frac{A_{dB}}{sin\alpha_B}\right)\right]B^2$	$\left[\rho_lA_l + \frac{1}{6}\rho_d\left(3\frac{A_{dD}}{sin\alpha_D} + \frac{A_{dB}}{sin\alpha_B}\right) + \frac{1}{6}\rho_s\left(3\frac{A_{sD}}{tan\alpha_D} + \frac{A_{sB}}{tan\alpha_B}\right)\right]B^2$
r_{do}	$\frac{1}{6}\rho_d\left(\frac{A_{dD}}{sin\alpha_D} + \frac{A_{dB}}{sin\alpha_B}\right)\Delta^2$	$\frac{1}{6}\rho_d\left(\frac{A_{dD}}{sin\alpha_D} + \frac{A_{dB}}{sin\alpha_B}\right)\Delta^2$
	Pattern 3	Pattern 4
Equivalent properties		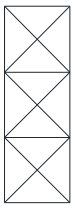
$(EA)_0$	$4E_lA_l + E_d(A_{dB}sin^3\alpha_B + A_{dD}sin^3\alpha_D)$	$4E_lA_l + E_d(A_{dB}sin^3\alpha_B + A_{dD}sin^3\alpha_D)$
$(GA_B)_0$	$4E_dA_{dB}sin\alpha_Bcos^2\alpha_B$	$4E_dA_{dB}sin\alpha_Bcos^2\alpha_B$
$(GA_D)_0$	$4E_dA_{dD}sin\alpha_Dcos^2\alpha_D$	$4E_dA_{dD}sin\alpha_Dcos^2\alpha_D$
$(GJ_x)_0$	$\frac{1}{4}((GA_B)_oD^2 + (GA_D)_oB^2)$	$\frac{1}{4}((GA_B)_oD^2 + (GA_D)_oB^2)$
$(\rho A)_0$	$4\left[\rho_lA_l + \rho_d\left(\frac{A_{dD}}{sin\alpha_D} + \frac{A_{dB}}{sin\alpha_B}\right)\right]$	$4\left[\rho_lA_l + \rho_d\left(\frac{A_{dD}}{sin\alpha_D} + \frac{A_{dB}}{sin\alpha_B}\right) + \frac{1}{2}\rho_s\left(\frac{A_{sD}}{tan\alpha_D} + \frac{A_{sB}}{tan\alpha_B}\right)\right]$
$(\rho J_x)_0$	$(\rho J_{xD})_o + (\rho J_{xB})_o$	$(\rho J_{xD})_o + (\rho J_{xB})_o$
$(\rho J_{xD})_0$	$\left[\rho_lA_l + \frac{1}{3}\rho_d\left(\frac{A_{dD}}{sin\alpha_D} + 3\frac{A_{dB}}{sin\alpha_B}\right)\right]D^2$	$\left[\rho_lA_l + \frac{1}{3}\rho_d\left(\frac{A_{dD}}{sin\alpha_D} + 3\frac{A_{dB}}{sin\alpha_B}\right) + \frac{1}{6}\rho_s\left(\frac{A_{sD}}{tan\alpha_D} + 3\frac{A_{sB}}{tan\alpha_B}\right)\right]D^2$
$(\rho J_{xB})_0$	$\left[\rho_lA_l + \frac{1}{3}\rho_d\left(3\frac{A_{dD}}{sin\alpha_D} + \frac{A_{dB}}{sin\alpha_B}\right)\right]B^2$	$\left[\rho_lA_l + \frac{1}{3}\rho_d\left(3\frac{A_{dD}}{sin\alpha_D} + \frac{A_{dB}}{sin\alpha_B}\right) + \frac{1}{6}\rho_s\left(3\frac{A_{sD}}{tan\alpha_D} + \frac{A_{sB}}{tan\alpha_B}\right)\right]B^2$
r_{do}	$\frac{1}{3}\rho_d\left(\frac{A_{dD}}{sin\alpha_D} + \frac{A_{dB}}{sin\alpha_B}\right)\Delta^2$	$\frac{1}{3}\rho_d\left(\frac{A_{dD}}{sin\alpha_D} + \frac{A_{dB}}{sin\alpha_B}\right)\Delta^2$

8. Conclusions

In the present research, a study was carried out of four spatial lattice patterns of rectangular cross-section, obtaining the elastic properties and equivalent inertias necessary for the representation of the problem as column-beam.

The proposed representation method, BC-FEM, based on the equivalent properties determined, has been validated numerically from comparing the results obtained in various case studies. From the results presented, the following conclusions can be deduced:

(1) The availability of a representation of lower complexity such as the beam-column formulation, reduces significantly the time needed for the model construction. This indicated formulation can be carried out from the equivalent properties determined in the research.

(2) The discretization of the geometry problem does not affect the performance of the static response of the model, even if the domain is represented by a single element. However, the dynamic response is affected by the discretization, but a $L_l/1$ ratio is sufficient to achieve adequate performance of the model. This robustness of the model allows a significant reduction in computational cost.

(3) Comparing the results of the different responses evaluated with the results obtained from the SL-FEM model, for a discretization of not less than $L_l/1$, the maximum difference found for the totality of the cases evaluated turned out to be less than 4 %.

(4) Being Δ a necessary parameter in the energy approach to obtain the equivalent properties, these determined properties showed excellent performance even for cases in which the $\Delta/side$ ratio was higher than the unit. This indicates the appropriate use of the BC model with these equivalent properties even for lattice cases with important diagonal spacing.

(5) The internal efforts that determine the structural behavior of each element of the spatial lattice (axial efforts), are easily recoverable from knowing in the BC-FEM model the forces acting at the height x of interest and applying the proposed analytical equations.

Acknowledgements

The authors are grateful for the financial support of the Universidad Tecnológica Nacional, Facultad Regional Mendoza, CeReDeTeC, (SeCyT, Project UTI6619TC).

References

[1] Abrate S., “Continuum modeling of lattice structures”, Shock and Vibration Digest, 17(1), 815-821, 1985.
[2] Abrate S., “Continuum modeling of lattice structures for dynamic analysis”, Shock and Vibration Digest, 20(10), 3-8, 1988.
[3] Noor A. and Mikulas M., “Continuum Modeling of Large Lattice Structures: Status and Projections”, In: Atluri S.N., Amos A.K. (eds.), Large Space Structures: Dynamics and Control. Springer Series in Computational Mechanics. Springer, Berlin, Heidelberg. 1988.
[4] McCallen D. and Romstad K., “A continuum model for the nonlinear analysis of beam-like lattice structures”, Computer and Structures, 29(2), 177-197, 1988.
[5] Filipich C. and Bambill E., “Natural frequencies of braced elements via power series”, In: AMCA (ed.), Macánica Computacional, 22, 877-891, 2003.
[6] Teughels A. and De Roeck G., “Continuum Modeling for beam-and platelike lattice structures”, Fourth International Colloquium on Computation of Shell {$\&$} Spatial Structures, IASSS-IACM 2000, Chania, Crete, Greece, 2000.
[7] Salehian A., “Micropolar Continuum Modeling of Large Space Structures with Flexible Joints and Thermal Effects: Theory and Experiment”, Ph.D. thesis, Virginia Polytechnic Institute and State University, 2008.
[8] Guzmán A., Rosales M. and Filipich C., “Natural vibrations and buckling of a spatial lattice structure using a continuous model derived from an energy approach”, International Journal of Steel Structures, 17(2), 565-578, 2017.
[9] Guzmán A., Rosales M. and Filipich C., “Continuous one-dimensional model of a spatial lattice. Deformation, vibration and buckling problems”, Engineering Structures, 182, 290-300, 2019.
[10] Madugula M., Wahba Y. and Monforton G., “Dynamic response of guyed mast”, Engineering Structures, 20(12), 1097-1101, 1998.
[11] Wahba Y., Madugula M. and Monforton G., “Evaluation of non-linear analysis of guyed antenna towers”, Computers and Structures, 68, 207-212, 1998.
[12] Ben Kahla N., “Equivalent beam-column analysis of guyed towers”, Computers and Structures, 55(4), 631-645, 1993.
[13] Páez P. and Sensale B., “Analysis of guyed masts by the stability functions based on the Timoshenko beam-column”, Engineering Structures, 152, 597-606, 2017a.
[14] Páez P. and Sensale B., “Cálculo de torres atirantadas sin utilizar elementos finitos”, Hormigón y Acero, 68(283), 229-240, 2017b.
[15] Computers and Structures, Inc. (CSI), SAP2000, 2007.